

Intercomparison of models representing direct shortwave radiative forcing by sulfate aerosols

O. Boucher,^{1,2} S. E. Schwartz,³ T. P. Ackerman,⁴ T. L. Anderson,⁵ B. Bergstrom,⁶ B. Bonnel,¹ P. Chýlek,⁷ A. Dahlback,^{8,9} Y. Fouquart,¹ Q. Fu,⁷ R. N. Halthore,³ J. M. Haywood,^{10,11,12} T. Iversen,¹³ S. Kato,^{4,14} S. Kinne,^{6,15} A. Kirkevåg,¹³ K. R. Knapp,¹⁶ A. Lacis,¹⁷ I. Laszlo,¹⁸ M. I. Mishchenko,¹⁷ S. Nemesure,³ V. Ramaswamy,¹¹ D. L. Roberts,¹⁰ P. Russell,⁶ M. E. Schlesinger,¹⁹ G. L. Stephens,¹⁶ R. Wagener,²⁰ M. Wang,⁷ J. Wong,⁷ and F. Yang¹⁹

Abstract. The importance of aerosols as agents of climate change has recently been highlighted. However, the magnitude of aerosol forcing by scattering of shortwave radiation (direct forcing) is still very uncertain even for the relatively well characterized sulfate aerosol. A potential source of uncertainty is in the model representation of aerosol optical properties and aerosol influences on radiative transfer in the atmosphere. Although radiative transfer methods and codes have been compared in the past, these comparisons have not focused on aerosol forcing (change in net radiative flux at the top of the atmosphere). Here we report results of a project involving 12 groups using 15 models to examine radiative forcing by sulfate aerosol for a wide range of values of particle radius, aerosol optical depth, surface albedo, and solar zenith angle. Among the models that were employed were high and low spectral resolution models incorporating a variety of radiative transfer approximations as well as a line-by-line model. The normalized forcings (forcing per sulfate column burden) obtained with the several radiative transfer models were examined, and the discrepancies were characterized. All models simulate forcings of comparable amplitude and exhibit a similar dependence on input parameters. As expected for a non-light-absorbing aerosol, forcings were negative (cooling influence) except at high surface albedo combined with small solar zenith angle. The relative standard deviation of the zenith-angle-averaged normalized broadband forcing for 15 models was 8% for particle radius near the maximum in this forcing ($\sim 0.2 \mu\text{m}$) and at low surface albedo. Somewhat greater model-to-model discrepancies were exhibited at specific solar zenith angles. Still greater discrepancies were exhibited at small particle radii, and much greater discrepancies were exhibited at high surface albedos, at which the forcing changes sign; in these situations, however, the normalized forcing is

¹Laboratoire d'Optique Atmosphérique, Université de Lille-I, Villeneuve d'Ascq, France.

²Formely at Laboratoire de Météorologie Dynamique du CNRS, Ecole Normale Supérieure, Paris, France.

³Environmental Chemistry Division, Brookhaven National Laboratory, Upton, New York.

⁴Meteorology Department, Pennsylvania State University, University Park.

⁵Joint Institute for the Study of the Atmosphere and the Oceans, University of Washington, Seattle.

⁶NASA Ames Research Center, Moffett Field, California.

⁷Atmospheric Science Program, Department of Physics, Dalhousie University, Halifax, Nova Scotia, Canada.

⁸Norwegian Institute for Air Research, Kjeller, Norway.

⁹Now at Department of Physics, University of Oslo, Oslo, Norway.

¹⁰Hadley Centre for Climate Prediction and Research, Meteorological Office, Bracknell, Berkshire, England, United Kingdom.

¹¹NOAA Geophysical Fluid Dynamics Laboratory, Princeton University, Princeton, New Jersey.

¹²Now at Meteorological Research Flight, Defence and Evaluation Research Agency, Farnborough, Hants, England, United Kingdom.

¹³Department of Geophysics, University of Oslo, Oslo, Norway.

¹⁴Now at Langley Research Center, Hampton, Virginia.

¹⁵Now at NASA Goddard Space Flight Center, Greenbelt, Maryland.

¹⁶Department of Atmospheric Science, Colorado State University, Ft. Collins.

¹⁷NASA Goddard Institute for Space Studies, New York.

¹⁸Department of Meteorology, University of Maryland, College Park.

¹⁹Department of Atmospheric Sciences, University of Illinois at Urbana-Champaign, Illinois.

²⁰Analytical Sciences Division, Brookhaven National Laboratory, Upton, New York.

Copyright 1998 by the American Geophysical Union.

Paper number 98JD00997.

0148-0227/98/98JD-00997\$09.00

quite small. Discrepancies among the models arise from inaccuracies in Mie calculations, differing treatment of the angular scattering phase function, differing wavelength and angular resolution, and differing treatment of multiple scattering. These results imply the need for standardized radiative transfer methods tailored to the direct aerosol forcing problem. However, the relatively small spread in these results suggests that the uncertainty in forcing arising from the treatment of radiative forcing of a well-characterized aerosol at well-specified surface albedo is smaller than some of the other sources of uncertainty in estimates of direct forcing by anthropogenic sulfate aerosols and anthropogenic aerosols generally.

1. Introduction

The direct radiative forcing due to scattering of solar radiation by anthropogenic sulfate aerosol has been suggested to be significant when compared to the longwave radiative forcing by anthropogenic greenhouse gases over the industrial period [Charlson *et al.*, 1991, 1992]. In early studies a relatively simple multiple reflection model was used to estimate this forcing on the basis of the atmospheric loading (column burden) of sulfate, but such estimates are subject to concern from the perspective of the accuracy of their representation of the radiative transfer. Issues for the radiative transfer calculation include sulfate scattering efficiency ($\text{m}^2 (\text{g sulfate})^{-1}$), aerosol upscatter fraction, dependence on surface albedo, dependence on wavelength, and multiple scattering effects. Penner *et al.* [1994] suggested that uncertainties involving the first three of these issues impose an uncertainty in direct climate forcing by sulfate aerosols of a factor of 1.6. Uncertainties arising from the latter two issues have not been assessed, but Kiehl and Briegleb [1993] suggested that initial estimates might be too great because of inadequate treatment of the wavelength dependence of the scattering efficiency. Other contributions to uncertainty in sulfate aerosol forcing include loading, geographical distribution, molecular form, interactions with other aerosol species, relative humidity effects, and for the indirect forcing the effects of added sulfate aerosol on cloud microphysics. Uncertainties in aerosol radiative forcing are thought to represent the greatest contribution to uncertainty in climate forcing over the industrial period [Intergovernmental Panel on Climate Change (IPCC), 1996; Schwartz and Andreae, 1996].

Several groups have recently addressed radiative forcing by sulfate aerosol [e.g., Pilinis *et al.*, 1995; Boucher and Anderson, 1995; Nemesure *et al.*, 1995], but significant unresolved differences remain. Comparison of these studies suggests that part of the difference may be due to the treatment of radiation; however, it is difficult to separate radiation model effects from other differences in approach. Boucher and Anderson [1995], using a global model, computed aerosol forcing for accumulation-mode sulfate aerosols. Nemesure *et al.*

[1995] reported forcing for column burdens of monodisperse sulfate aerosols. Pilinis *et al.* [1995] reported forcing for a "global mean" aerosol consisting of fine and coarse modes. Consequently, it is difficult to infer separately the effects of differences in cloud and surface albedo, aerosol size distributions employed, and the like.

In view of the importance of the climate forcing due to aerosols, in general, and sulfate aerosols, in particular, and the resultant need to identify and reduce uncertainties in forcing estimates, it is considered desirable to ascertain and explain the extent of the differences in these estimates. Here we take an initial step in this direction by means of an intercomparison by several groups conducting independent calculations. The participants in this intercomparison project are listed in Table 1; the characteristics of the models they used are briefly outlined in Table 2. A total of 21 different sets of calculations were submitted for comparison from 12 different groups and involving 15 different radiative transfer models, albeit several of them closely related. Several of the codes are used in general circulation models (GCMs) at present, whereas some are too detailed to be used in GCMs because of constraints on computing time.

There is some precedent for an intercomparison of shortwave radiation codes. Fouquart *et al.* [1991] intercompared shortwave radiation codes for climate studies as part of the Intercomparison of Radiation Codes in Climate Models (ICRCCM) activity [Ellingson and Fouquart, 1991]. Several cases involving aerosols were reported. Examination of the published paper and unpublished results (Y. Fouquart, personal communication, 1996) indicates that the top-of-atmosphere (TOA) forcing due to changes in aerosol optical depth differed substantially in magnitude and even in sign for the several models. For the case of maritime aerosol (single scattering albedo of 0.99, optical depth 0.09, and surface albedo 0.20) the relative standard deviation for 11 models examined was 23% for solar zenith angle (SZA) 75° and 114% for SZA 30° , with three of the models in the latter case exhibiting a slight positive aerosol forcing. The reasons for the large discrepancies are not clear and apparently have not been extensively pursued subsequent to that intercomparison.

Table 1. List of Participants, Affiliations, and Acronyms

Participants	Group	Affiliation
R. N. Halthore, S. Nemesure, S. E. Schwartz, and R. Wagener	BNL	Brookhaven National Laboratory, Upton, New York
K. R. Knapp and G. L. Stephens	CSU	Colorado State University, Ft. Collins
P. Chýřtek, Q. Fu, M. Wang, and J. Wong	Dalhousie	Dalhousie University, Halifax, Nova Scotia, Canada
J. M. Haywood and V. Ramaswamy	GFDL	NOAA Geophysical Fluid Dynamics Laboratory, Princeton University, Princeton
T. L. Anderson and O. Boucher	LMD/UW	Laboratoire de Météorologie Dynamique, Paris, France University of Washington, Seattle
B. Bonnel and Y. Fouquart	LOA	Laboratoire d'Optique Atmosphérique, Université de Lille, Villeneuve d'Ascq, France
B. Bergstrom, S. Kinne, and P. Russell	NASA Ames	NASA Ames Research Center, Moffett Field, California
A. Lacis and M. I. Mishchenko	NASA GISS ¹	NASA Goddard Institute of Space Studies, New York
A. Dahlback, T. Iversen, and A. Kirkevåg	Oslo	University of Oslo, Oslo, Norway Norwegian Institute for Air Research, Kjeller, Norway
T. P. Ackerman and S. Kato	PSU	Pennsylvania State University, University Park
M. E. Schlesinger and F. Yang	UIUC	University of Illinois at Urbana-Champaign
J. M. Haywood and D. L. Roberts	UKMO	United Kingdom Meteorological Office, Bracknell, Berkshire, England, United Kingdom
I. Laszlo	UMD	University of Maryland, College Park

¹This group participated only in intercomparison of Mie aerosol properties (see Figures 2d and A2).

2. Description of the Calculations

In order to restrict the sources of discrepancy in the several calculations to differences in treatment of optical properties and radiative transfer and thereby to permit characterization of the magnitude of discrepancy arising only from differing treatments of these processes the present intercomparison specified a rather prescriptive set of conditions for the calculations to be conducted by the participating groups. These conditions are presented here. It should be noted, however, that the conditions specified for the present intercomparison are not meant to reflect actual conditions, which can vary considerably from those specified here and which can therefore lead to rather different estimates of the forcing for a given sulfate loading. Actual assessments of radiative forcing by sulfate aerosols would need to take such variable conditions into account, and of course, differing assumptions about these conditions and differing representations by different groups can be expected to contribute to further uncertainty in estimates of radiative forcing by sulfate aerosol than is indicated in the present rather restrictive intercomparison.

2.1. Aerosol Composition

The aerosol composition was specified to be that of an ammonium sulfate solution at 80% relative humidity (deliquescence point or saturated solution) and 25°C. The specified index of refraction was $1.40-0.00i$ for the purpose of these calculations, independent of wavelength [*Tang and Munkelwitz*, 1991]. Sulfate mass per particle was evaluated as sulfate concentration in solution (g sulfate m^{-3} solution) times particle volume (cubic meters). The sulfate concentration for the saturated solution corresponds to 540 g ammonium sulfate L^{-1} of solution at 25°C [*Tang and Munkelwitz*, 1994] equivalent to $(96/132)$ g sulfate (g ammonium sulfate) $^{-1} * 540$ (g ammonium sulfate L^{-1}) * 1000 ($L m^{-3}$) = $3.927 \cdot 10^5$ g sulfate m^{-3} .

2.2. Size Distribution

Forcing was calculated for specified values of particle radius with a narrow size distribution in order to avoid complications arising from high-frequency Mie resonances. Since the possible differences from model to model may result from different choices of size distribution most participants used a lognormal size distribution with standard deviation $\sigma_0 = 0.1$ (Sometimes the lognormal size distribution is expressed in terms of the geometric standard deviation $\sigma_g = \exp(\sigma_0) = 1.10517$ in this specific case.) Forcing was calculated for aerosols having the radius values (mode or geometric mean) specified in Table 3. This mass was calculated for the nominal particle radius rather than for the specific size distribution employed; for the lognormal size distribution with $\sigma_0 = 0.1$ this underestimates particle mass by 4.6%. These radius values, which are in a geomet-

Table 2. Characteristics of the Mie Codes and Radiative Models Used in the Intercomparison Project

Label	Mie Code	Solving Method	Number of Streams of Bands	Number of Bands	Width of the 550 nm Band	Gasous Absorption	References
◇	BNL-AD	Hansen and Travis [1974] adding-doubling	12	7	exact	{ 30% absorption based on Coakley et al. [1983]	Nemesure et al. [1995]
◆	BNL-6S	Vermote et al. [1997] successive orders of scattering	N/A	1520 ¹	2.5 nm	HITRAN 82	Vermote et al. [1997]
△	CSU ²	Wiscombe [1979] two-stream delta-Eddington	2	6	N/A	Fu and Liou [1992]	Stackhouse and Stephens [1991]
◁	Dalhousie	Bohren and Huffman [1983] delta-four stream	4	6 ³	exact	{ H ₂ O, O ₂ , CO ₂ ¹ HITRAN 82 O ₃ : Howard et al. [1961]	{ Fu and Liou [1992] Fu and Liou [1993]
▲	GFDL	Bohren and Huffman [1983] adding-doubling ⁴	16	LBL ⁵	1 cm ⁻¹	HITRAN 92	Ramaswamy and Freidenreich [1991]
×	LMD/UW-Sunray ²	Kattawar and Plass [1967] two-stream Eddington	2	2	N/A	Pade approximants, HITRAN 82	Fouquart and Bonnel [1980]
×	LMD/UW-Streamer	Kattawar and Plass [1967] discrete-ordinate method ⁴	12	24	50 nm	Tsay et al. [1989]	Key [1994] and Stamnes et al. [1988]
+	LOA-DOM ⁶	discrete-ordinate method	12	208	12.08 nm	HITRAN 92	See Section 4
▽	LOA-Z ⁶	two-stream	2	208	12.08 nm	HITRAN 92	Zdankowski et al. [1980]
○	NASA-Ames	Dave [1969] adding-doubling	12	8	100 nm	LOWTRAN 5	Plass et al. [1973]
□	Oalo ²	Based on Wiscombe [1980] six-stream ⁴	6	16	N/A	O ₃ only H ₂ O, O ₂ , CO ₂ HITRAN 92 H ₂ O continuum.	Stamnes et al. [1988]
■	PSU	Toon and Ackerman [1981] delta two-stream	2	32	17.1 nm	Clough and Iacono [1995]	{ Toon et al. [1989] Kato et al. [1997]
*	UIUC	{ Based on Twomey [1977] and Liou [1989] two-stream delta-Eddington	2	3 ⁷	250 nm	{ H ₂ O Chou [1986] O ₃ Lacis and Hansen [1974] CO ₂ Fouquart and Bonnel [1980]	Oh [1989]
●	UKMO	Bohren and Huffman [1983] two-stream delta-Eddington	2	4	2 nm	{ O ₃ LOWTRAN 7 Other gases HITRAN 92	{ Edwards and Slingo [1996] Haywood et al. [1997b]
△	UMD ⁶	Wiscombe [1979] adding-doubling	16	193	15 nm	LOWTRAN 7	{ Laszlo [1994] Wiscombe et al. [1984]

N/A, "Not Applicable", LOWTRAN 5, Kneizys et al. [1980], LOWTRAN 7, Kneizys et al. [1988], HITRAN 82, Rothman et al. [1983], and HITRAN 92, Rothman et al. [1992]

¹Results were scaled up by a factor of 1.00875 to account for radiation outside wavelength region 0.25–4.0 μm

²These models are not included in the comparisons of the 550 nm partial forcings

³The first band (0.2–0.7 μm) is divided into 10 subintervals where the spectral dependences of O₃ absorption and aerosol optical properties have been considered explicitly.

⁴These models used the Henyey-Greenstein approximation to the phase function in lieu of the Mie phase function

⁵LBL, line-by-line, because of computational requirements, this model was run only in a limited number of cases for the broadband forcing.

⁶These models included a background aerosol: a maritime aerosol model with optical depth 0.075 in the LOA models and a continental aerosol model with optical depth 0.23 in the UMD model.

⁷The k-distribution method with 6 k intervals has been used to compute the water vapor absorption in the third band (0.69–4.0 μm), and Rayleigh scattering is neglected in the third band

Table 3. Sulfate Mass Per Particle for Particle Radii Used in This Study

Radius, μm	Sulfate Mass, 10^{-15} g sulfate per particle
0.03000	0.04442
0.04243	0.1256
0.06000	0.3553
0.08485	1.005
0.1200	2.843
0.1697	8.040
0.2400	22.74
0.3394	64.32
0.4800	181.9
0.6788	514.6
0.9600	1455

Data are for ammonium sulfate and relative humidity of 80%.

ric progression increasing by a factor of $2^{1/2}$, span the range of interest for forcing by accumulation-mode particles. Figure 1 shows the corresponding distributions for $\sigma_0 = 0.1$. It is seen that the widths of the distributions are comparable to the spacing of the successive distributions. The increasing width with increasing radius corresponds to a constant fractional width (i.e., constant width on a logarithmic radius scale). Results for monodisperse size distributions and other size distributions such as the gamma distribution [Hansen and Travis, 1974; Lacis and Mishchenko, 1995] are discussed in the appendix.

2.3. Aerosol and Atmospheric Optical Properties

Aerosol scattering cross-section σ (m^2 per particle), phase function, asymmetry parameter, etc., corresponding to above aerosol properties were evaluated by each group according to its practice. The incremental aerosol was to be placed in the boundary layer for those models which accommodated such vertical resolution. Atmospheric absorptive properties (including column water vapor) were employed in calculations by each group according to its practice. The atmospheric profile corresponds to midlatitude summer; most participants used the midlatitude summer profile from McClatchey *et al.* [1972]. One series of calculations was carried out at a fixed surface albedo, $R_s = 0.15$, for the following values of optical depth at 550 nm τ_{550} (0.05, 0.10, 0.15, 0.20, 0.30, 0.40, 0.50, and 0.60). A second series of calculations held aerosol optical depth fixed at $\tau_{550} = 0.20$ and varied surface albedo R_s over the following values (0.05, 0.10, 0.15, 0.20, 0.25, 0.30, 0.40, 0.60, and 0.80). The surface reflectance function was treated by each group according to its practice.

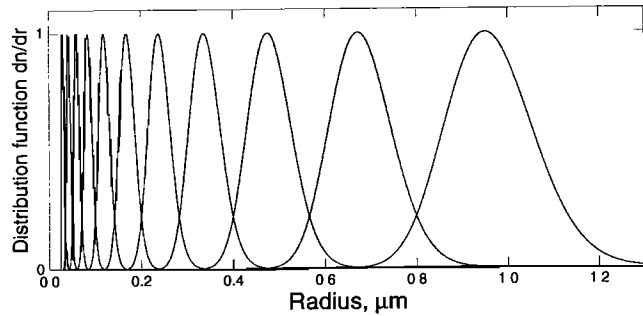


Figure 1. Distribution functions employed in the calculations of aerosol scattering efficiency and forcing. Distribution functions are displayed on a linear scale. The increasing width on a linear scale corresponds to a constant width on a logarithmic scale. Distributions are normalized to equal maximum values.

2.4. Definition of Aerosol Forcing

The direct aerosol forcing due to sulfate aerosols, ΔF , was calculated as the change in the net solar flux at TOA when the sulfate aerosol is included in the model atmosphere relative to that when the sulfate aerosol was absent [IPCC, 1996]. No account is made for stratospheric adjustment; in any event, the changes in upper tropospheric and stratospheric heating rates due to the inclusion of sulfate aerosols will be small. Two groups included a “background” aerosol; the Laboratoire d’Optique Atmosphérique (LOA) and the University of Maryland (UMD) groups used the maritime-I (MAR-I) and continental-I (CONT-I) aerosol models of the standard radiation atmospheres [World Climate Research Programme, 1983], respectively. According

Table 4. Values of the Cosine of the Solar Zenith Angles and Corresponding Weights Used to Compute Global Mean Forcing

μ_0	W_i
0.0092	0.0472
0.0479	0.1069
0.1150	0.1601
0.2063	0.2032
0.3161	0.2335
0.4374	0.2491
0.5626	0.2491
0.6839	0.2335
0.7937	0.2032
0.8850	0.1601
0.9521	0.1069
0.9908	0.0472

See equations (1)–(3).

Table 5. Summary of the Eight Cases Selected for Statistical Analysis

Case	Optical Depth τ	Surface Albedo R_s	SZ SZA	Particle Radius $r_0, \mu\text{m}$	Broadband Forcing			550 nm Partial Forcing		
					Median, W g^{-1}	Range, %	Standard Deviation, %	Median, $\text{W g}^{-1} \text{nm}^{-1}$	Range, %	Standard Deviation, %
1	0.2	0.15	Ave.	0.042	-42.3	145	31	-0.087	47	13
2	0.2	0.15	Ave.	0.170	-443.5	27	8	-1.03	38	12
3	0.2	0.15	Ave.	0.679	-318.6	50	12	-0.57	28	11
4	0.2	0.05	Ave.	0.170	-548.4	26	8	-1.27	36	12
5	0.2	0.80	Ave.	0.170	-26.0	613	193	-0.063	108	29
6	0.2	0.15	83.4°	0.170	-634.0	75	20	-1.46	97	32
7	0.2	0.15	71.6°	0.170	-1183	34	11	-2.85	54	17
8	0.2	0.15	7.8°	0.170	-679.0	44	14	-1.33	67	26

SZA is solar zenith angle. Ave. is average and refers to the zenith-angle-averaged forcing as defined in equation (4).

to the above definition, forcing is generally a negative quantity because sulfate aerosol is non-light-absorbing. Two steps are involved in the computation of aerosol forcing ΔF . First, wavelength-dependent aerosol optical properties are computed as a function of size and composition for the values of τ_{550} given previously. Second, radiative forcing is computed by the use of a multiple scattering radiative transfer algorithm. Each group treated the integration over the solar spectrum according to its practice.

Participants were also requested to calculate forcings at a specific wavelength, $\lambda = 550$ nm (partial forcing $d\Delta F/d\lambda$ in $\text{W m}^{-2} \text{nm}^{-1}$), when this was possible with the model employed. For this calculation the extraterrestrial solar spectral irradiance at 1 AU and 550 nm, $dF_0/d\lambda$, was specified as $1.884 \text{ W m}^{-2} \text{nm}^{-1}$ [Neckel and Labs, 1984]. For groups representing the solar spectrum as a set of broadband intervals the partial forcing at 550 nm was calculated as the forcing for the interval encompassing 550 nm divided by the width of that interval in nanometers, and the results were scaled to the same spectral irradiance. The intent of this calculation was to isolate the effects on forcing arising from different treatments of the solar spectrum from those arising from the different treatment of radiative transfer or optical properties.

Forcing ΔF and partial forcing $d\Delta F/d\lambda$ were evaluated for the values of cosine of solar zenith angle μ_0 given in Table 4. These values are selected to permit integration by a 12-point Gaussian quadrature to evaluate the global mean forcing [Hansen and Travis, 1974; Press et al., 1988]. The global average forcing (half the average over the illuminated hemisphere) is calculated as the integral over the cosine of solar zenith angle μ_0 :

$$\overline{\Delta F} = \frac{1}{2} \int \Delta F d\mu_0 \quad (1)$$

with the integral approximated as

$$\int \Delta F d\mu_0 = \frac{1}{2} \sum_i \Delta F(\mu_{0,i}) W_i \quad (2)$$

where the weights W_i correspond to globally and annually averaged solar illumination and are given in Table 4. Note that the weights are normalized to $\sum_i W_i = 2$ and $\sum_i \mu_{0,i} W_i = 1$ so that

$$\overline{\Delta F} = \frac{1}{4} \sum_i \Delta F(\mu_{0,i}) W_i \quad (3)$$

Forcings are reported as normalized forcings G calculated as forcing divided by sulfate column burden, in units of W m^{-2} per g sulfate m^{-2} (i.e., $\text{W (g sulfate)}^{-1}$) for the broadband forcing, and $\text{W (g sulfate)}^{-1} \text{nm}^{-1}$ for the partial forcing.

3. Results

To characterize the spread in forcing as calculated by the several groups we selected eight cases, summarized in Table 5, for which we provide statistics. The statistics characterize the results from 15 models for the broadband forcing and 12 models for the 550 nm partial forcing for three different aerosol radii (cases 1–3), three different surface albedos (cases 2, 4, and 5) (all for zenith-angle averages), and three different solar zenith angles (cases 6–8). Table 5 shows medians of the forcing values, the range of the results (difference between the largest and the smallest values expressed as percent of the median value), and the standard deviation from the mean (expressed as percent of the mean value). Also presented are results from a model that employed a line-by-line representation of atmospheric molecular absorption over the solar spectrum.

The intercomparison reveals a considerable spread in the normalized aerosol forcings for the 8 specific cases of Table 5. Note that for case 5, the high surface albedo case, the range is very large, reflecting the fact that the models disagree even on the sign of the forcing, as discussed in section 3.5. Even with exclusion of this case the range of the broadband normalized forcing for the several models is systematically $>25\%$ and considerably greater for the smallest normalized forcings. The stan-

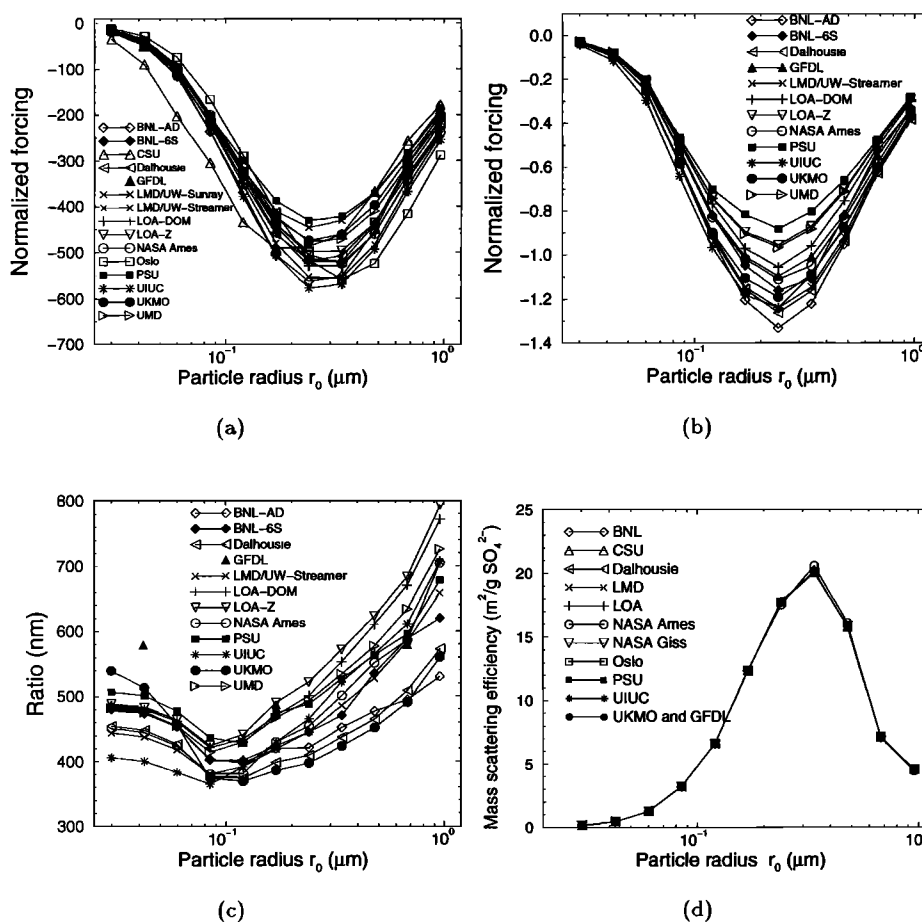


Figure 2. (a) Broadband normalized forcing (W m^{-2} per g sulfate m^{-2} or $\text{W (g sulfate)}^{-1}$) as a function of particle radius. Aerosol optical depth $\tau_{550} = 0.2$ and surface albedo $R_s = 0.15$. (b) Narrowband partial forcing at 550 nm ($\text{W m}^{-2} \text{ nm}^{-1}$ per g sulfate m^{-2} or $\text{W (g sulfate)}^{-1} \text{ nm}^{-1}$) as a function of particle radius for the conditions specified in Figure 2a. (c) Ratio of the broadband to the partial forcing (nanometers). The dependency of mass scattering efficiency at 550 nm with particle radius is shown concurrently in (d). The forcings are zenith-angle averages (i.e., calculated according to (4)).

standard deviation is generally $>8\%$ and is as great as 30% (case 1, particle radius $r_0 = 0.042 \mu\text{m}$). The standard deviation is considerably less for the partial normalized forcing at 550 nm than that for the broadband forcing in case 1 but is not appreciably reduced for the other zenith-angle-averaged cases (2–4) and somewhat surprisingly is actually considerably greater than that for the broadband forcing for specific solar zenith angles (cases 6–8). It should be noted that this last conclusion holds also for just the 12 models that provided narrowband forcing, establishing that these differences in cases 6–8 are not due simply to outliers in the broadband only models. The line-by-line model predicts normalized forcings which are not systematically greater or smaller than those for other models and are very close to the median values for the partial forcings. The results of the calculations are presented in Figures 2–6 and discussed below in terms of the dependence of the normalized forcing on particle radius, aerosol optical depth, surface albedo, and solar zenith angle.

3.1. Sensitivity to Particle Radius

The dependence of forcing on particle radius as calculated by the several groups is shown in Figures 2a and 2b for the broadband forcing and the 550 nm partial forcing, respectively. The maximum in broadband forcing occurs for radius of $\sim 0.2\text{--}0.4 \mu\text{m}$, depending on the model. (In using the term maximum when referring to a negative quantity such as forcing we refer to the maximum of the absolute value of the quantity). Compared to the “average” results, the maximum in broadband forcing is shifted toward a smaller radius for the Colorado State University (CSU) model and toward a larger radius for the Oslo model and to a lesser extent for the NASA Ames model. In the Oslo model, gaseous absorption by CO_2 , O_2 , and water vapor is not included; this would tend to overestimate the downward solar flux reaching the aerosol layer and probably the aerosol forcing for particle sizes closest to the absorption wavelengths of CO_2 and H_2O . There is a range of

~40% among the several models in the magnitude of the maximum normalized forcing. The dependence of the normalized forcing on particle radius is due mainly to the dependence of mass scattering efficiency on particle radius as seen in Figure 2d with some additional dependence on aerosol phase function as particle size increases [e.g., Schwartz, 1996]. Figure 2d shows a fair consistency in the scattering efficiency ($\text{m}^2 (\text{g sulfate})^{-1}$) calculated by the several groups reproducing the conventional [e.g., Ouimette and Flagan, 1982] maximum in this efficiency at a particle diameter approximately equal to the wavelength of the light. The range of maximum values for the mass scattering efficiency varies between 20.06 and 20.6 $\text{m}^2 (\text{g SO}_4^{2-})^{-1}$ with a mode maximum of 20.1 $\text{m}^2 (\text{g SO}_4^{2-})^{-1}$. This divergence is attributed to differences in the Mie codes employed by the several groups but may also be due to a lack of precision in the calculations. The normalized forcings exhibit a substantially greater spread (Figure 2a) than do the scattering efficiencies (Figure 2d). This indicates that the spread in forcing results from differences in the treatment of the radiative transfer rather than in the evaluation of the aerosol scattering efficiency.

The radius dependence of the partial forcing is slightly more sharply peaked than that of the broadband forcing with the maximum in partial forcing occurring at a slightly lower radius. In this respect the 550 nm wavelength is not representative of the total solar spectrum. Somewhat surprisingly, the maximum in partial forcing (12 models) exhibited just as great a range as for the broadband forcing (15 models). This indicates that the spread in broadband forcing arises mainly from differing treatments of the radiative transfer problem rather than from different representations of the solar spectrum. Nonetheless, generally speaking, there is a better agreement among the models regarding the shape of the curves (Figure 2b), with all the models indicating a maximum at essentially the same radius value.

Further insight into the radius dependence of forcing can be gained from the ratio of the broadband to the partial forcing (Figure 2c). This forcing ratio is not independent of radius although it is considerably more slowly varying than either of the forcings themselves. For most models the forcing ratio exhibits a minimum (i.e., the ratio of partial to broadband forcing exhibits a maximum), consistent with a more peaked radius dependence for the partial forcing than for the broadband forcing, as driven mainly by the fact that the maximum in scattering efficiency depends on the ratio of radius to wavelength. The minimum in forcing ratio occurs at a particle radius of $\sim 0.1 \mu\text{m}$, somewhat lower than the radius of maximum scattering efficiency.

It is important to note at this stage that the sensitivity of forcing to particle radius would be smaller in the case of a "real" aerosol distribution with a larger standard deviation [Boucher and Anderson, 1995] than is indicated in these comparisons with narrow size distributions. Therefore, to some extent the differences in radius dependence shown here would be washed out in

integrations over a broad aerosol size distribution and may thus be an exaggeration of the model-to-model differences. Nonetheless, because the normalized forcings for the several distributions more or less maintain their relative positions at different radius values (Figure 2a), the spread in normalized forcing for a broad aerosol size distribution for the several models would be comparable to that indicated for the narrow distributions near the maximum forcing (i.e., relative standard deviation of $\sim 10\%$).

3.2. Sensitivity to Optical Depth

The sensitivity of normalized forcing to aerosol optical depth is examined in Figures 3a–3c for the broadband forcing and 3d–3f for the partial forcing at 550 nm. At any given optical depth, at intermediate particle sizes the range among the models is roughly 25%–30% for the broadband normalized forcing and 30%–40% for the partial normalized forcing. Because the quantity plotted is the normalized forcing, that is the forcing per sulfate column burden, and because the optical depth scales linearly with sulfate column burden, a linear dependence of forcing on optical depth would be represented in these plots by a straight line parallel to the x axis. The fractional deviation from such a horizontal line represents the departure from such a linear dependence. In all cases the magnitude of the normalized forcing decreases monotonically with increasing optical depth over the range examined, 0.05–0.6, with the exception of the Laboratoire de Météorologie Dynamique (LMD) / University of Washington (UW) Sunray model for the broadband forcing at small optical depths. The decrease in broadband normalized forcing over this optical depth range is 13%–21% for intermediate particle sizes, where the normalized forcing is largest.

It may be observed that the maximum of nonlinear dependence of forcing on optical depth (i.e., the maximum of the derivative of the broadband normalized forcing with respect to optical depth) occurs at the lowest values of optical depth. This may be understood by considering the forcing to be proportional to $(\exp(-\tau) - 1)$. Taylor series expansion of this quantity yields the normalized forcing proportional to $-1 + \tau/2 - \tau^2/6 + \tau^3/24 + \dots$. This functional dependence is shown in Figure 3e for several values of the intercept of normalized partial forcing at 550 nm versus τ_{550} for which the wavelength of the forcing corresponds to the wavelength at which the optical depth is specified. Quite close agreement is indicated between the limiting slopes from the several models and the limiting slopes resulting from this analysis. However, the decrease in the slope with increasing τ is larger in the model results than predicted from this simple analysis.

3.3. Sensitivity to Surface Albedo

We present the dependence of normalized global average forcing on surface albedo in Figures 4a and 4b for the broadband and partial forcings, respectively. It is

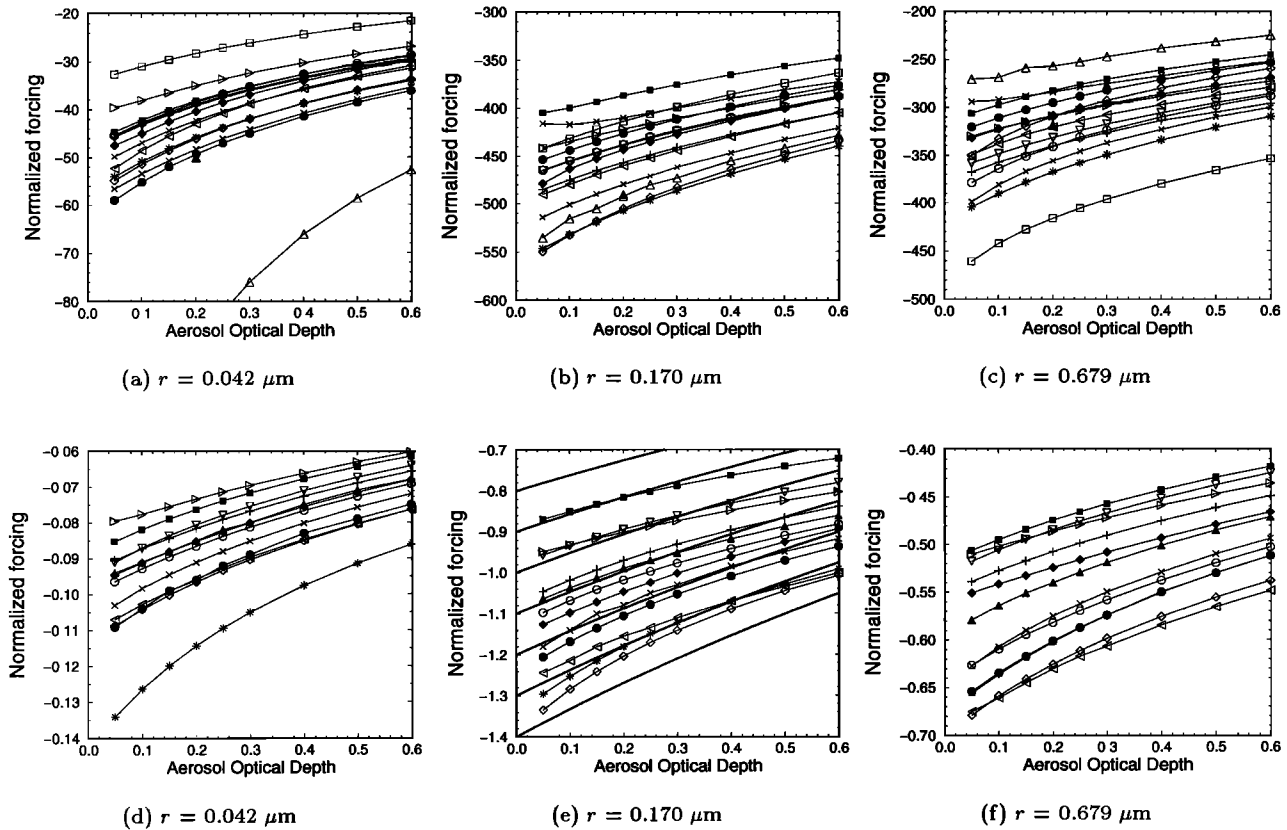


Figure 3. (a), (b), and (c) Broadband normalized forcing (W (g sulfate^{-1})) as a function of optical depth for three different particle radii. (d), (e), and (f) Idem for the 550 nm partial forcing (W ($\text{g sulfate}^{-1} \text{ nm}^{-1}$)). The limiting slopes are shown in Figure 3e as bold lines for different normalized forcings at the origin (see text). The forcings are zenith-angle averages for surface albedo $R_s = 0.15$. Symbols denoting the several models are as in Figure 2 and Table 2.

seen that the (absolute) forcing decreases with increasing surface albedo, as expected for a scattering aerosol above an increasingly bright surface. All the models display this dependence to fairly close agreement, although the relative departure becomes increasingly great at high surface albedo. To examine this more closely, we make use of an approximation by *Charlson et al.* [1991], which is based on multiple reflections between the aerosol and the surface. According to this approximation, aerosol forcing is linear in $(1 - R_s)^2$. Figures 4c and 4d show the broadband and partial normalized forcings as a function of $(1 - R_s)^2$, exhibiting approximate linearity. To test this approximation further, we plotted graphs of forcing divided by $(1 - R_s)^2$, which should be independent of R_s within the above approximation (see Figures 4e and 4f). The approximation is supported fairly well for all models up to $R_s = 0.2$. The increase in (absolute) forcing divided by $(1 - R_s)^2$ with R_s indicates that aerosol forcing does not decrease with R_s as fast as the above approximation would suggest. There is also substantial divergence (positive or negative) from this approximation for some models, especially for $R_s > 0.4$, which can be found over snow or when the aerosol is above a cloud layer. The approximation holds somewhat better for the 550 nm

partial forcing, suggesting that the departure of the several models arises from differences in treatment of atmospheric absorption.

3.4. Dependence of Forcing on Solar Zenith Angle

Knowledge of the dependence of aerosol forcing on solar zenith angle is essential for several reasons. First, the zenith-angle-averaged forcing assumes uniform geographic distribution of aerosol loading and properties as well as other properties that influence aerosol light scattering such as surface albedo, cloud cover, and relative humidity, a situation that is never achieved in the real world. Mapping the geographic distribution of aerosol forcing requires explicit consideration of seasonal and latitudinal distribution of SZA [*Wagner et al.*, 1994; *Nemesure et al.*, 1995]. Likewise, investigation of the relation between the secular decrease in temperature diurnal range and increase in aerosol forcing [*Karl et al.*, 1993] requires consideration of the diurnal variations of the aerosol forcing (and hence its SZA dependence). Finally, the influence on aerosol forcing of diurnal variations in quantities like relative humidity, cloud cover, and surface albedo cannot be examined with a zenith-angle-averaged forcing.

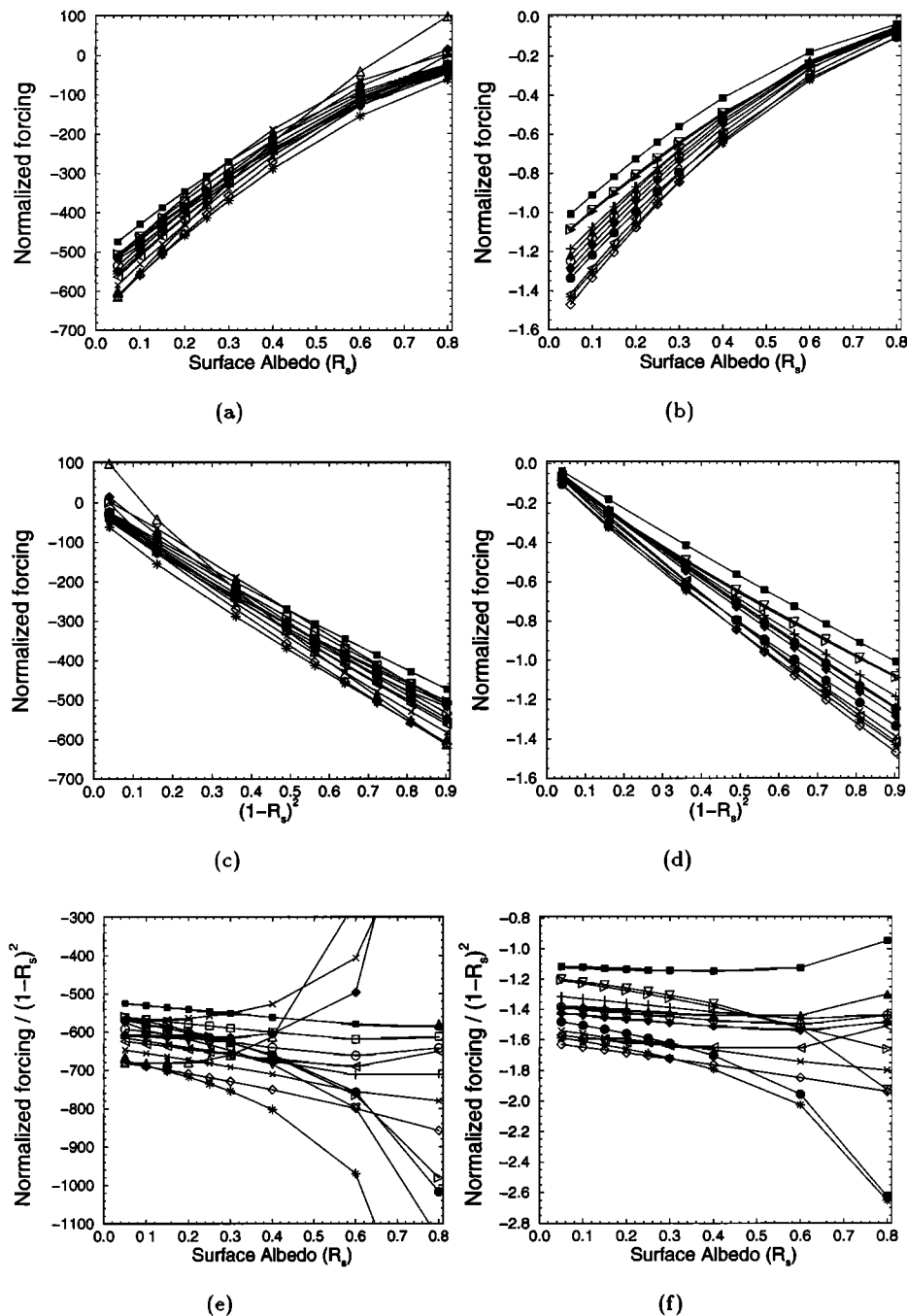


Figure 4. (a) Broadband normalized forcing as a function of surface albedo, R_s , (c) broadband normalized forcing as a function of $(1 - R_s)^2$, and (e) broadband normalized forcing divided by $(1 - R_s)^2$ as a function of R_s . (b), (d), and (f) Idem for the 550 nm partial forcing. The forcings are zenith-angle averages for an optical depth $\tau_{550} = 0.2$ and particle radius $r_0 = 0.17 \mu\text{m}$. Symbols denoting the several models are as in Figure 2 and Table 2.

The dependence of aerosol forcing with SZA may be understood qualitatively [Nemesure *et al.*, 1995; Schwartz, 1996] to result from a near cancellation of two effects for an optically thin atmosphere: the increase in the slant path aerosol optical depth ($\tau/\cos(\text{SZA})$) with increasing SZA and the decrease in incident solar flux ($S \cos(\text{SZA})$) with increasing SZA. The cancellation of

these two effects results in the amount of the direct beam flux that is scattered by aerosols being nearly independent of SZA. The optically thin approximation no longer holds at large SZA, so the aerosol forcing goes to zero at large SZA. At small SZA the SZA dependence of aerosol forcing (i.e., the upscattered flux) depends mainly on the phase function of the aerosol and,

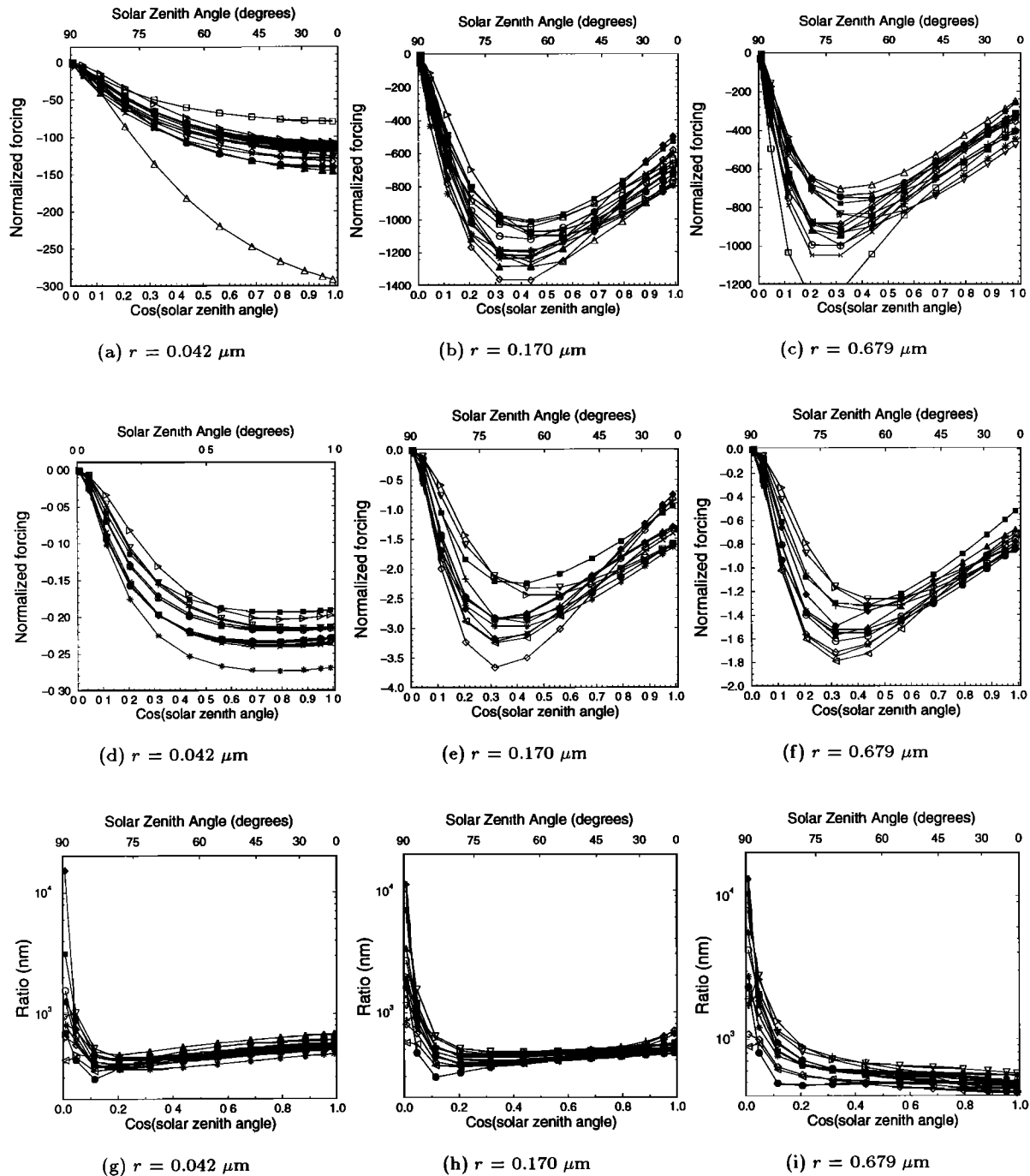


Figure 5. (a), (b), and (c) Broadband normalized forcing (W (g sulfate^{-1})) as a function of solar zenith angle for three different particle radii. (d), (e), and (f) Idem for the 550 nm partial forcing (W ($\text{g sulfate}^{-1} \text{ nm}^{-1}$)). (g), (h), and (i) Ratio of the broadband to the 550 nm forcing at the three different radii (nanometers). The forcings are for an optical depth of $\tau_{550} = 0.20$ and surface albedo $R_s = 0.15$. Symbols denoting the several models are as in Figure 2 and Table 2.

in turn, on particle size. At small radii (i.e., for particles near the Rayleigh limit of Mie scattering) the phase function is nearly symmetric, so the forcing weakens as SZA increases from zenith to horizon as governed by increased Rayleigh scattering (Figures 5a and 5d). For larger particles the scattering phase function is increasingly peaked in the forward direction; this results in a

low upscatter fraction for small SZA that increases with increasing SZA, resulting in an increase in forcing with increasing SZA until, finally, the aerosol scattered flux decreases because the slant path is no longer optically thin. This leads to aerosol forcing going through a maximum at intermediate SZA (Figures 5b and 5e; 5c and 5f).

As shown in Figure 5, all the models succeed in capturing these features. Some of the differences among the models (see Figures 5a to 5f) are caused by use of different phase functions. *Boucher* [1998] showed that for a given aerosol size distribution and refractive index, using an equivalent Henyey-Greenstein phase function instead of the original Mie phase function (which is accurate but computationally more intensive) may cause errors in aerosol forcing as great as 20%. Some groups (e.g., LMD/UW with “Streamer” and GFDL with the line-by-line model) computed the asymmetry factor with Mie theory and used the corresponding Henyey-Greenstein phase function, whereas other groups (e.g., LOA) expanded the phase function in Legendre polynomials thereby gaining a better approximation of the original Mie phase function. The Henyey-Greenstein phase function does a poor job of predicting upscatter fractions at small and large SZA, but errors somewhat cancel out in the average over SZA [*Wiscombe and Grams, 1976; Boucher, 1998*]. This distinction among the models is not applicable for the two-stream models for which the asymmetry factor is usually the only parameter by which the phase function is characterized.

The ratios of the broadband to the 550 nm forcings are displayed in Figures 5g, 5h, and 5i. We can think of this ratio as a measure of the importance of the 550 nm wavelength for the broadband forcing. Large ratios indicate that other wavelengths (either smaller or larger than 550 nm) contribute to a larger proportion to the direct radiative forcing than the 550 nm wavelength region. As solar zenith angle increases, the larger wavelengths become more and more important at the expense of the smaller ones because of the λ^{-4} dependence of Rayleigh scattering. Depending on whether the particle radius is smaller (Figures 5g and 5h) or larger (Figure 5i) than the reference wavelength of 550 nm the ratio goes through a minimum or increases steadily with SZA. These results show that the 550 nm forcing can definitely not be used as a surrogate for the broadband forcing, even for a first-order calculation of aerosol direct forcing. Moreover, the discrepancies among the models are very high.

3.5. Positive Forcing at High Surface Albedo

A striking result from this study is the finding of a positive aerosol forcing (for a nonabsorbing aerosol) under the conditions of high surface albedo and small SZA (Figure 6). The magnitude of the positive forcing at small SZA is comparable to that of negative forcing at large SZA; the zenith-angle-averaged forcing, evaluated by (3), remains negative (Figure 4). These features are exhibited by all the models for both the broadband and the partial forcings, albeit with substantial differences in detail. Such positive forcing has previously been noted by several investigators [e.g., *Herman and Browning, 1975*], but no explanation was provided. Because this positive forcing is found also at the 550 nm

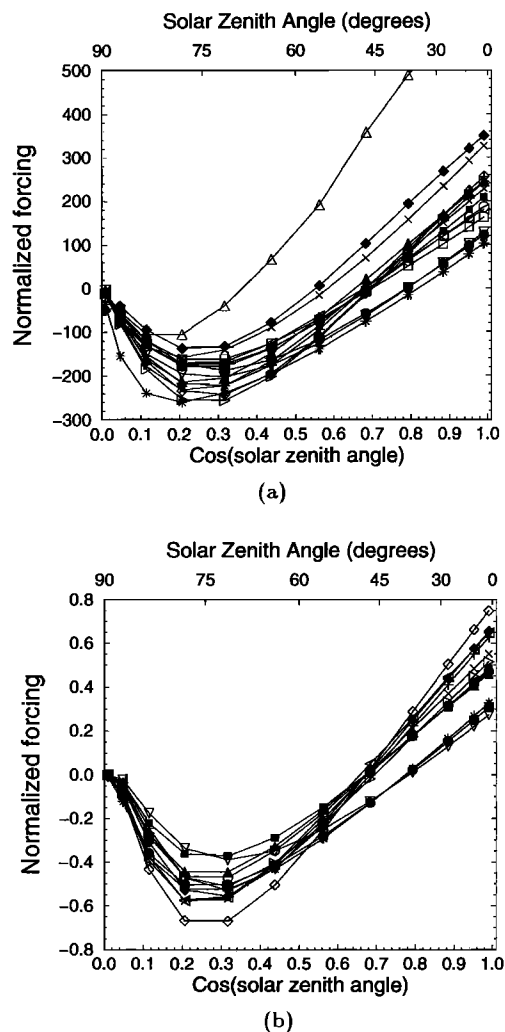


Figure 6. (a) Broadband and (b) 550 nm partial forcing as function of solar zenith angle for surface albedo 0.60. The forcings are for an aerosol optical depth $\tau_{550} = 0.20$ and particle radius $r_0 = 0.170 \mu\text{m}$. Symbols denoting the several models are as in Figure 2 and Table 2.

wavelength, where there is no gaseous absorption, and because the aerosol is nonabsorbing, the reason for this enhanced absorption due to the presence of the aerosols is to be sought at the surface rather than in the atmosphere. An explanation has been provided recently by *Haywood and Shine* [1997]. When the sun is at zenith, the downwelling solar irradiance that is reflected upward is proportional to aerosol optical depth, but the upwelling irradiance that is reflected back to the surface is proportional to the optical depth multiplied by the average photon path length through the aerosol layer (i.e., $5/3$ times the optical depth for a Lambertian surface). With some assumptions, *Haywood and Shine* [1997] used a simple reflection model to derive an inequality for the onset of positive forcing:

$$\frac{5}{3} R_s^2 - \frac{8}{3} R_s + 1 < 0 \quad (\text{i.e., } R_s > 0.6) \quad (4)$$

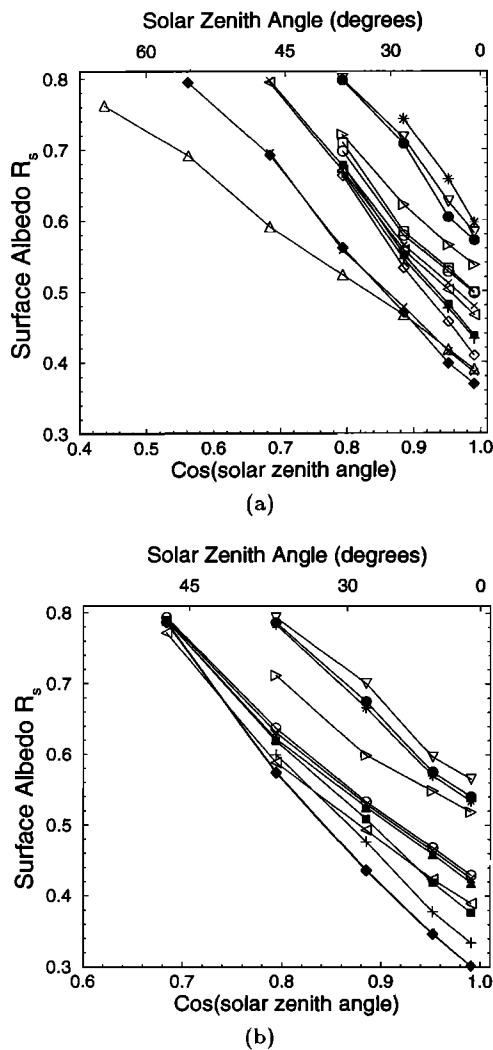


Figure 7. Values of cosine of the solar zenith angle, $\cos(\theta_0)$, and surface albedo, R_s , corresponding to the onset of positive forcing; forcing is positive for $\cos(\theta_0)$ and R_s above and to the right of the locus of points indicated for the several models: (a) broadband forcing and (b) partial forcing. Data are for an aerosol optical depth $\tau_{550} = 0.20$ and particle radius $r_0 = 0.170 \mu\text{m}$. Symbols denoting the several models are as in Figure 2 and Table 2.

The range of surface albedo for which a positive forcing is found depends on solar zenith angle (see Figure 7). Some models simulate positive forcings for surface albedo as low as 0.3 or solar zenith angles as large as 45° . For some values of surface albedo and SZA the models also disagree on the sign of the forcing (Figures 7 and 6). It should be noted that conditions where the surface reflectance is high and the solar zenith angle is small occur over a relatively small proportion of the Earth's surface, making this phenomenon relatively unimportant in estimates of global aerosol forcing. Although it might be argued that a significant positive forcing may occur if scattering aerosol exists above a highly reflectant cloud, column calculations performed

for such conditions by *Haywood and Shine* [1997] did not reveal any positive radiative forcing. Additionally, the global calculations performed by *Haywood et al.* [1997b] using the United Kingdom Meteorological Office (UKMO) radiative transfer code employed in the present intercomparison did not show any areas of positive radiative forcing in monthly means.

4. Approximate Representations of Spectral Dependence of Aerosol Forcing

Because radiative transfer with high spectral resolution models is computationally intensive, it is important to develop and test the accuracy of methods for approximating the broadband aerosol forcing by means of low spectral resolution models. Calculations by the LMD/UW group examined an approach to this that is based on a preliminary averaging of aerosol optical properties. In these calculations (denoted Streamer nwd) the wavelength variation of aerosol optical properties is compressed into two spectral intervals (i.e., the spectral intervals corresponding to the LMD/UW-Sunray model, $0.25\text{--}0.68 \mu\text{m}$ and $0.68\text{--}4 \mu\text{m}$) by weighted averages over relevant portions of the solar spectrum, the mass scattering coefficient being weighted by the solar flux at the surface, and the asymmetry parameter being weighted by the product of the solar flux and the mass scattering efficiency. These results were compared to the results obtained in a reference set of calculations (denoted Streamer and displayed throughout Figures 2–6), which employed aerosol optical properties computed at the midpoints of the 24 bands. In this way the difference caused by averaging aerosol optical properties was investigated without changing the spectral resolution of the model itself. Figure 8 shows the ratio of the broadband normalized forcings from these two calculations. Averaging the aerosol optical properties results in

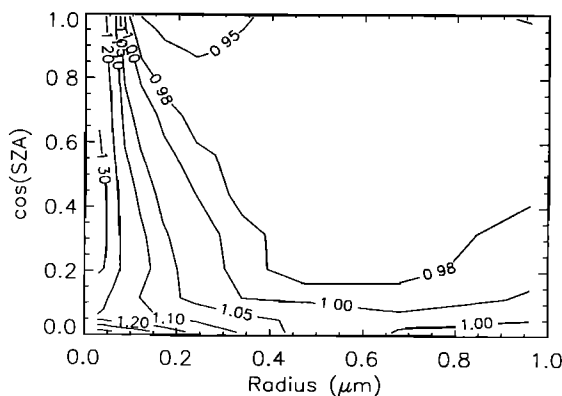


Figure 8. Ratio of broadband normalized forcings computed with the Streamer model (LMD-UW group) for a spectrally averaged (2 bands) and a spectrally resolved (24 bands) representation of aerosol optical properties. Surface albedo is 0.15, and aerosol optical depth is 0.20.

quite accurate results for larger particles ($r > 0.1 \mu\text{m}$) for which optical properties are only weakly dependent on wavelength but in somewhat greater errors, 20%–30%, for small particles close to the Rayleigh regime ($r < 0.075 \mu\text{m}$) but for which the normalized forcing is in any event quite small.

The treatment of spectral variation in aerosol optical properties was also examined by the Dalhousie group. The broadband normalized forcings were calculated with different procedures prescribing aerosol spectral optical properties (Figure 9). In “Dalhousie-mid,” aerosol optical properties at midpoints of the six spectral bands were used. In “Dalhousie-mean,” spectrally averaged aerosol optical properties weighted by solar irradiance were obtained over each of the six spectral bands. For results denoted as “Dalhousie” and displayed in Figures 2–6 the spectral variation of aerosol

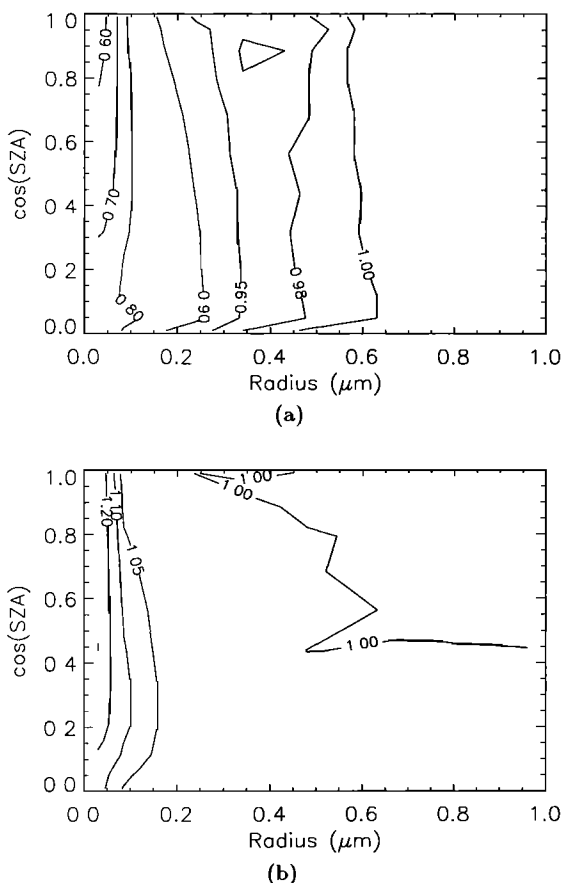


Figure 9. Ratio of the broadband normalized forcings computed by the Dalhousie group with different procedures for prescribing aerosol spectral optical properties. (a) Ratio of forcing calculated with the Dalhousie-mid model (aerosol properties calculated at mid points of six spectral bands) to that calculated with the reference Dalhousie model (aerosol properties calculated as means in 15 spectral bands); (b) ratio of forcing calculated with the Dalhousie-mean model (aerosol properties calculated as means in six spectral bands) to that calculated with the reference Dalhousie model. Surface albedo is 0.15, and aerosol optical depth is 0.20.

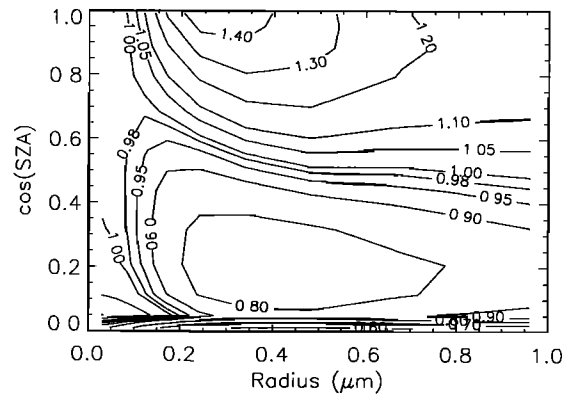


Figure 10. Ratio of the broadband normalized forcings computed by the LOA group with the two-stream Zdunkowski method (LOA-Z) to those calculated by the discrete-ordinate method (LOA-DOM) with same spectral resolution. Surface albedo is 0.15, and aerosol optical depth is 0.20.

optical properties was treated in the same way as in the Dalhousie-mean except that the first spectral band ($0.2\text{--}0.7 \mu\text{m}$) is further divided into 10 subintervals. The errors are substantial (up to 40%) for the smallest particles when midpoint optical properties are used (see Figure 9a). By using spectrally averaged optical properties in the first band ($0.2\text{--}0.7 \mu\text{m}$), errors in forcings are reduced but can still be as large as 25% for the smallest particle radii (Figure 9b). As with the LMD/UW approach, the approximate techniques yielded forcings that closely approximated forcings obtained with the more detailed spectral model for large particle radii.

The LOA group computed the broadband normalized forcings with two different solving methods (two-stream method in LOA-Z and discrete-ordinate method in LOA-DOM) but with the same spectral resolution. Figure 10 indicates an overestimation of aerosol forcing by the two-stream method at small solar zenith angles and an underestimation at large solar zenith angles with some dependence on radius as well. However, the differences between the two radiative codes are much smaller for global-average forcings. Taken together, the results from these studies suggest that it is possible to compute aerosol forcing to a reasonable accuracy with a low spectral resolution model, provided aerosol optical properties are suitably averaged (e.g., weighted by TOA solar irradiance) and aerosol particles are not too small.

5. Discussion and Conclusions

In principle the calculation of radiative forcing by sulfate aerosols should, for prescribed conditions, be a completely solved problem. In practice, there are approximations and assumptions that must inevitably be introduced into any calculation of this forcing that will result in errors in the resultant calculated forcing.

These assumptions and approximations include treatment of the solar spectrum and molecular absorption spectrum of the atmosphere, surface reflectance including its angular and spectral dependence, size distribution of the aerosol, angular dependence of light scattering by aerosols, multiple scattering, and the vertical distribution of atmospheric components. The present exercise is an attempt to estimate the errors in such calculations resulting from assumptions and approximations in modeling the forcing by comparing the results of different groups using somewhat different approaches to these calculations for well-specified aerosol properties and surface reflectance. Comparison of the results of these calculations indicates that for globally-averaged direct forcing by accumulation-mode aerosols ($0.170\ \mu\text{m}$ radius, near the maximum in scattering efficiency) over surfaces of low albedo (0.05–0.15) the standard deviation of normalized forcing calculated by 15 models is 8% (range 26%–27%). For 12 models for which it was possible to evaluate the partial forcing at 550 nm the corresponding standard deviation is 12% (range 36%–38%). Although the models employed are not wholly independent, still these results suggest that errors resulting from differing approximations and assumptions in the treatment of aerosol optics and radiative transfer contribute an uncertainty in estimates of aerosol direct radiative forcing of $\sim 20\%$ (twice the standard deviation). Moreover, there is consistency among virtually all the models in the dependence of forcing on the examined variables: particle radius (Figure 2), optical depth (Figure 3), surface albedo (Figure 4), and solar zenith angle (Figures 5 and 6). The models likewise all exhibited similar departure from linear dependence of forcing on aerosol optical depth and on $(1 - R_s)^2$ suggested by simple models [Charlson *et al.*, 1991]. These findings suggest that uncertainties resulting from modeling aerosol optics and radiative transfer contribute relatively little to the overall uncertainty associated with climate forcing by atmospheric aerosols.

There are several reasons, however, why this tentative conclusion might be questioned. Detailed comparison of the models as a function of any of the several controlling variables indicates considerably greater departure than is implied by the 8% standard deviation. One notes first that the partial forcing at 550 nm, not requiring integration over wavelength, might be expected to exhibit closer agreement than the broadband forcing. Yet this is found only for the globally-averaged forcing when the broadband only models are excluded from the statistics, while the opposite is found at specific solar zenith angles. Future work might therefore focus on the spectral dependence of the forcing and possible compensating errors. Likewise, the spread in forcing was greater at any specific solar zenith angle than in the zenith-angle average, again indicative of possible fortuitous compensating errors in the several models (Figures 5b and 5e). With respect to dependence of forcing on particle radius, again, although the several models all showed a

similar overall dependence, at extremes of particle radius the normalized forcing for the several models exhibited a relative spread that was much greater than at radii for which the scattering efficiency and normalized forcing were the greatest. Finally, the marked divergence of the models at high surface reflectivity suggests that work must be done to understand the reasons for these discrepancies if confidence is to be placed in the ability of models to treat these situations. Fortunately, from the perspective of inferring climate forcing by such aerosols these discrepancies would appear to be of somewhat secondary importance, although they can be of considerable importance in specific situations. Comparison of the spread in the optical calculations (scattering efficiency) with that in the radiative calculations indicates that the spread in forcing results from differences in the treatment of the radiative transfer (such as multiple scattering) and treatment of the solar spectrum rather than in evaluation of the aerosol scattering efficiency.

With respect to the evaluation of aerosol forcing in climate models, from the results summarized in Table 5 it can be seen that with the exception of case 5 (surface reflectance 0.80) the spread of the results, albeit significant, is moderate. This suggests that coarse spectral resolution radiative transfer codes within GCMs are unlikely to produce large errors in direct radiative forcing. Generally speaking, we note that the simpler models (two-stream models, such as LMD/UW–Sunray, LOA-Zdunkowski method (LOA-Z), Pennsylvania State University (PSU), and UKMO, which are more likely to be used in GCMs) tend to exhibit smaller forcings than more elaborate models (such as LMD/UW–Streamer and LOA-Discrete Ordinate Method (LOA-DOM) using the discrete ordinate method, Brookhaven National Laboratory (BNL–AD), Geophysical Fluid Dynamics Laboratory (GFDL), and NASA Ames using the adding-doubling method, and BNL–6S using the method of successive orders of scattering). However, this generalization does not hold entirely. The University of Illinois at Urbana-Champaign (UIUC) model with the two-stream delta-Eddington method predicts aerosol forcings on the high side. The UMD model with the adding-doubling method predicts aerosol forcings on the low side but would probably be on the high side if no background aerosol was included.

The spread of results indicated in the present study is significantly less than that which can be inferred from the very limited examination of aerosol radiative influences in the 1991 ICRCCM intercomparison as noted in section 1. The relative standard deviations noted there (23% for SZA 75° and 114% for SZA 30°) may be most closely compared to cases 7 and 8 in the present study (11% for SZA 71.6° and 14% for SZA 7.8°). The reasons for this improvement are not apparent, but it should be noted that aerosol forcing had not been an explicit objective of the ICRCCM activity and had to be inferred from the unpublished calculations as the dif-

ference between different model runs having different aerosol loading. Still, we are pleased at the apparent improvement in model intercomparability between that study and the present one.

With respect to possible future resolution of the model-to-model differences indicated in the present study, unfortunately, such resolution is not amenable to experimental investigation, which would require characterization of the aerosol (including its vertical distribution), the surface reflectance (including its angular distribution and wavelength dependence), and the top-of-the-atmosphere radiative flux that is well beyond present capability. However, certain aspects of model results can still be examined in field studies. For example, during the recent Tropospheric Aerosol Radiative Forcing Observational Experiment (TARFOX) the direct radiative forcing due to a predominantly scattering aerosol was found to increase with increasing solar zenith angle (P. Hignett and J. P. Taylor, personal communication, 1997); such a dependence was exhibited by all the models participating in the present project. Such measurements provide at least a comforting qualitative confirmation of model performance but certainly not the ability to resolve differences among the models. It is necessary to develop and implement ways to test the various other features of the model calculations, such as dependence of the forcing on aerosol optical depth, surface albedo, solar zenith angle, and wavelength, if not to provide quantitative confirmation of model performance, at least for identifying important features that might be missed by the models.

We were unable to identify any of the models that could be viewed as the most likely approximation of an absolute reference method since, as noted, all the models embody approximations and assumptions. We would like to address the question of what would constitute a “benchmark” radiative transfer model for determination of the direct radiative forcing of aerosols. Such a model necessarily requires verified Mie calculations, high spectral resolution, use of the full Mie-calculated phase function, accurate treatment of the angular dependence of multiple scattering, accurate treatment of the molecular scattering and absorption, and sufficient vertical resolution. At present, none of the models used here possess all of the attributes listed above. There are only a few models used in this study which capture several but not all of these features in a highly precise manner. With respect to future calculations we would hope that the present data set can provide a useful basis of comparison for such a benchmark model and also for future parametrizations that might be suitable for inclusion in GCMs.

With respect to the broader issue of uncertainty in estimates of global average direct forcing by aerosol such as are listed by Penner *et al.* [1994] an additional uncertainty appears to be the calculation of forcing with a radiative transfer model even once all the input parameters are specified. This uncertainty amounts to some 20% (i.e., an uncertainty factor of 1.2 in the ter-

minology of Penner *et al.*), as evidenced in this study by intercomparison of several state-of-the-art models. For comparison, propagation of the several uncertainties listed by Penner *et al.* [1994] leads to an estimate of an overall uncertainty factor of 2.3. The dominant sources of uncertainty result from estimates of the loading of sulfate aerosol, controlled by atmospheric chemistry and deposition, for which estimates are available only from atmospheric chemistry models [e.g., Langner and Rodhe, 1991; Pham *et al.*, 1995; Kasibhatla *et al.*, 1997]. Additional major uncertainties arise from uncertainty and variability in aerosol size distribution [e.g., Boucher and Anderson, 1995] and the representation of the effects of spatial and temporal variations in relative humidity [Nemesure *et al.*, 1995; Haywood *et al.*, 1997a] and fractional cloud amount [Haywood *et al.*, 1997a]. In this context it seems clear from the present study that uncertainty deriving from treatment of the optical and radiative components of the aerosol forcing, for specified aerosol properties and surface albedo, contributes relatively little to the overall uncertainty in sulfate aerosol forcing and that major reduction of the overall uncertainty will require reduction in the larger uncertainties in the input parameters of radiative calculations.

Appendix: Dependence of Scattering Efficiency on Particle Size Distribution Function

As described above, we initially requested calculations for a narrow but not monodisperse size distribution with the object of diminishing sensitivity to high-

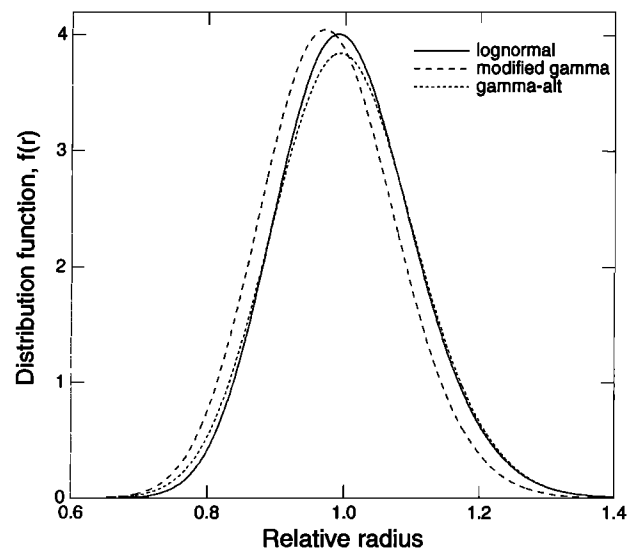


Figure A1. Comparison of lognormal and modified gamma distributions. Note that the modified gamma distribution with nominal parameters identical to that for the lognormal distribution is shifted to slightly smaller radius values. The “gamma-alt” distribution calculated for parameters a and b equal to the effective radius and effective variance of the lognormal distribution much more closely overlaps that distribution. Distributions are normalized to equal area.

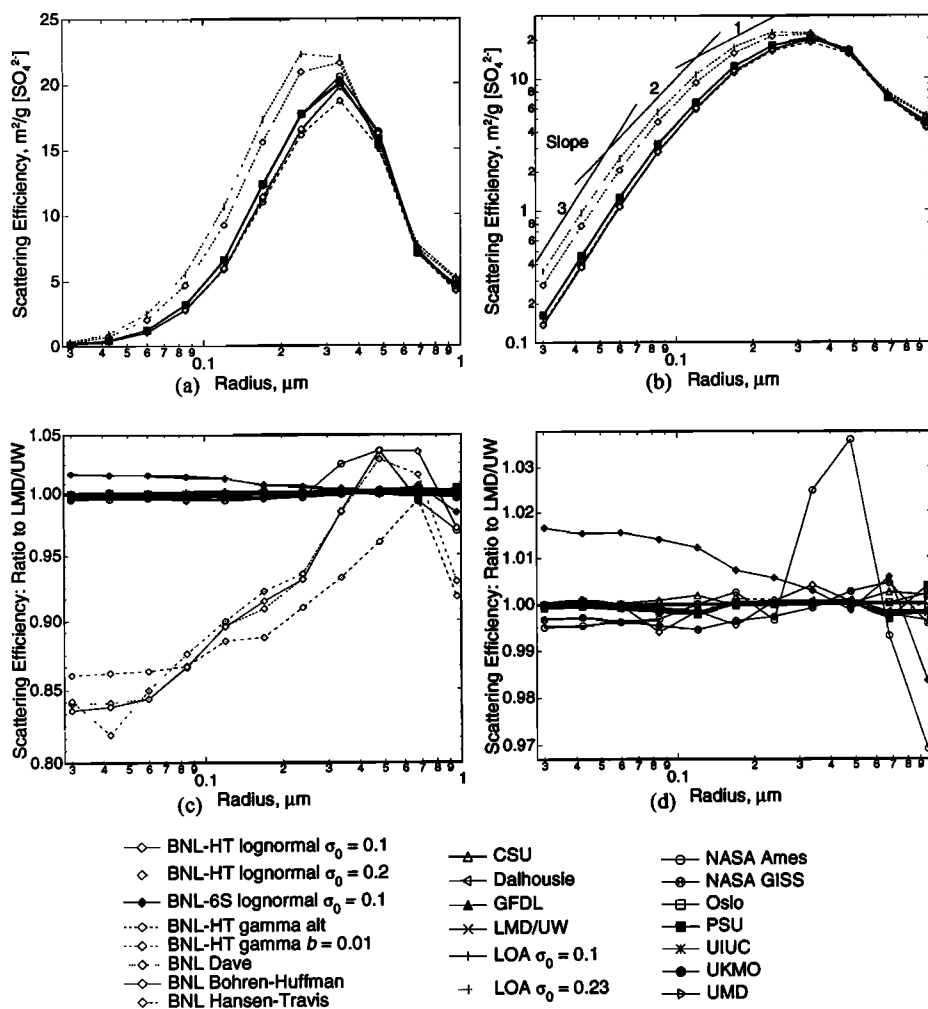


Figure A2. (a) Radius dependence of scattering efficiency ($\text{m}^2 (\text{g sulfate})^{-1}$) at wavelength 550 nm for all submitted calculations. Note the departure for lognormal calculations for $\sigma_0 = 0.20$ and 0.23 (compared to those for $\sigma_0 = 0.1$) showing sensitivity to that parameter. (b) Same as Figure A2a but on a logarithmic scale. Also shown for comparison are line segments having slopes of 3 (Rayleigh regime) and 2 and 1 (Mie scattering). (c) Ratio of scattering efficiency to that of the LMD/UW calculation on expanded logarithmic scale to show the magnitude of spread among the several calculations. Results for $\sigma_0 = 0.2$ and 0.23 are omitted here. Results for BNL-6S were for $\sigma_0 = 0.09$, resulting in the slight offset; radiative transfer calculations were made and reported for the cross sections shown. (d) Same as Figure A2c but with further expansion and omission of results for BNL-Hansen-Travis, BNL-Dave, BNL-Bohren-Huffman, and BNL-gamma distribution with variance = 0.01.

frequency Mie resonances. Results from the several groups revealed an unanticipated sensitivity to the details of the size distribution (Figure A1). Here we report findings regarding this sensitivity of the scattering efficiency to properties of the narrow distributions.

The lognormal distribution is given by

$$n(r) = dN/dr = \frac{1}{\sqrt{2\pi} \sigma_0 r} \exp \left[-\frac{(\ln r - \ln r_g)^2}{2\sigma_0^2} \right] \quad (\text{A1})$$

Sensitivity to the standard deviation σ_0 was examined in calculations by the BNL group ($\sigma_0 = 0.1$ and 0.2) and the LOA group ($\sigma_0 = 0.1$ and 0.23). As seen in Figure A2a, the use of the broader distributions leads to substantially greater scattering efficiencies by as much

as a factor of 1.7 and 2.1, respectively. This sensitivity apparently arises from the steep slope of the dependence of the scattering efficiency on r especially at low values of r (Figure A2b). Figures A2c and A2d further illustrate the departures by showing on an expanded scale the ratio of scattering efficiency to that obtained by the LMD/UW group. This sensitivity to the width of the size distribution, even for narrow size distributions as employed here, underscores the importance of careful specification of the size distribution in any such calculations and in any comparisons of calculations to measurements. The dependence of the scattering efficiency on shape of the distribution employed was examined further by the BNL group, who examined the scattering efficiency also for the modified gamma distribution

$$n(r) = dN/dr = \frac{(ab)^{(2b-1)/b}}{\Gamma[(1-2b)/b]} r^{(1-3b)/b} e^{-r/(ab)} \quad (\text{A2})$$

For the distribution written in this form [Hansen and Travis, 1974; Lacis and Mishchenko, 1995], a and b are equal to the effective radius r_e and the effective variance v_e where the latter quantities are defined as

$$r_e = \frac{\int_0^\infty r \pi r^2 n(r) dr}{\int_0^\infty \pi r^2 n(r) dr} \quad (\text{A3})$$

$$v_e = \frac{\int_0^\infty (r - r_e)^2 \pi r^2 n(r) dr}{r_e^2 \int_0^\infty \pi r^2 n(r) dr} \quad (\text{A4})$$

In calculations by the BNL group (BNL-gamma $b = 0.01$), a was set equal to the nominal radius r_g of the several calculations as given in Table 3, and b was taken as 0.01. Although the distribution functions are closely matched (Figure A1), the resulting scattering efficiencies are as much as 16% lower than those for the lognormal distribution with the same nominal parameters. This is attributed to the distribution's being shifted to a slightly lower radius. To examine this further, a modified gamma distribution (BNL-gamma alt) was constructed where the parameters a and b were selected to be equal to the effective radius and effective variance, respectively, of the lognormal distribution having $\sigma_0 = 0.1$. Aerosol scattering efficiencies predicted with this size distribution and with the corresponding lognormal size distribution were essentially identical (Figures A2c and A2d). As seen in Figure A1, this distribution also much more closely matches the lognormal distribution than does the modified gamma distribution with nominal values, confirming the attribution of the difference in scattering efficiency to the slight shift in distributions.

Several algorithms for calculating Mie scattering properties of monodisperse distributions were also examined, specifically those of Bohren and Huffman [1983], Hansen and Travis [1974], and Dave [1969]. These distributions also yielded scattering efficiencies that were lower than those for the lognormal distributions at low radii where the scattering efficiency exhibits a strong dependence on radius.

Because of the dependence of scattering efficiency on the distribution function employed, comparisons of forcing were restricted to identical distribution functions, namely, the lognormal distribution with $\sigma_0 = 0.1$. Although the sensitivity to the details of the distribution affects any calculations for narrow test distributions, such as were employed in the present intercomparison, it does not affect to such an extent calculations for realistic broad aerosol size distributions, as would pertain to ambient aerosols [Boucher and Anderson, 1995].

Acknowledgments. Work by CSU was done as part of the AT722 (Atmospheric Radiation and Energetics) class at the Department of Atmospheric Sciences at CSU. Work at BNL was supported by the Environmental Sciences Di-

vision of the U.S. Department of Energy (DOE) as part of the Atmospheric Radiation Measurement Program and was performed under the auspices of DOE under contract DE-AC02-98CH10886. Work at UKMO was supported by the UK Department of Environment, Transport and the Regions under contract PECD/7/12/37. The authors thank K. Shine for his thorough review.

References

- Bohren, C. F., and D. R. Huffman, *Absorption and Scattering of Light by Small Particles*, John Wiley, New York, 1983.
- Boucher, O., On Aerosol direct radiative forcing and the Henyey-Greenstein phase function, *J. Atmos. Sci.*, **55**, 128–134, 1998.
- Boucher, O., and T. L. Anderson, GCM assessment of the sensitivity of direct climate forcing by anthropogenic sulfate aerosols to aerosol size and chemistry, *J. Geophys. Res.*, **100**, 26,117–26,134, 1995.
- Charlson, R. J., J. Langner, H. Rodhe, C. B. Leovy, and S. G. Warren, Perturbation of the northern hemisphere radiative balance by backscattering from anthropogenic sulfate aerosols, *Tellus, Ser. AB*, **43**, 152–163, 1991.
- Charlson, R. J., S. E. Schwartz, J. M. Hales, R. D. Cess, J. A. Coakley, J. E. Hansen, and D. J. Hofmann, Climate forcing by anthropogenic aerosols, *Science*, **255**, 423–430, 1992.
- Chou, M. D., Atmospheric solar heating rate in the water vapor bands, *J. Clim. Appl. Meteorol.*, **25**, 1532–1542, 1986.
- Clough, S. A., and M. J. Iacono, Line-by-line calculation of atmospheric fluxes and cooling rates, 2, Application to carbon dioxide, ozone, methane, nitrous oxide and the halocarbons, *J. Geophys. Res.*, **100**, 16,519–16,535, 1995.
- Coakley, J. A., R. D. Cess, and F. B. Yurevich, The effects of tropospheric aerosols on the Earth's radiation budget: A parameterization for climate models, *J. Atmos. Sci.*, **40**, 116–138, 1983.
- Dave, J. V., Scattering of visible light by large water spheres, *Appl. Opt.*, **8**, 155–164, 1969.
- Edwards, J. M., and A. Slingo, Studies with a flexible new radiation code, I, Choosing a configuration for a large-scale model, *Q. J. R. Meteorol. Soc.*, **122**, 689–719, 1996.
- Ellingson, R. G., and Y. Fouquart, The intercomparison of radiative codes in climate models: An overview, *J. Geophys. Res.*, **96**, 8925–8927, 1991.
- Fouquart, Y., and B. Bonnel, Computations of solar heating of the Earth's atmosphere: A new parameterization, *Contrib. Atmos. Phys.*, **53**, 35–62, 1980.
- Fouquart, Y., B. Bonnel, and V. Ramaswamy, Intercomparing shortwave radiation codes for climate studies, *J. Geophys. Res.*, **96**, 8955–8968, 1991.
- Fu, Q., and K. N. Liou, On the correlated k -distribution method for radiative transfer in nonhomogeneous atmospheres, *J. Atmos. Sci.*, **49**, 2139–2156, 1992.
- Fu, Q., and K. N. Liou, Parameterization of the radiative properties of cirrus clouds, *J. Atmos. Sci.*, **50**, 2008–2025, 1993.
- Hansen, J. E., and L. D. Travis, Light scattering in planetary atmospheres, *Space Sci. Rev.*, **16**, 527–610, 1974.
- Haywood, J. M., and K. P. Shine, Multi-spectral calculations of the direct forcing of tropospheric sulphate and soot aerosols using a column model, *Q. J. R. Meteorol. Soc.*, **123**, 1907–1930, 1997.
- Haywood, J. M., V. Ramaswamy, and L. J. Donner, A limited-area-model case study of the effects of subgrid scale variations in relative humidity and cloud upon the

- direct radiative forcing of sulfate aerosol, *Geophys. Res. Lett.*, *24*, 143–146, 1997a.
- Haywood, J. M., D. L. Roberts, A. Slingo, J. M. Edwards, and K. P. Shine, General circulation model calculations of the direct radiative forcing by anthropogenic sulphate and fossil-fuel soot aerosol, *J. Clim.*, *10*, 1562–1577, 1997b.
- Herman, B. M., and S. R. Browning, The effect of aerosols on the Earth-atmosphere albedo, *J. Atmos. Sci.*, *32*, 1430–1445, 1975.
- Howard, J. N., J. I. F. King, and P. R. Gast, Thermal radiation, in *Handbook of Geophysics*, chap. 16, 16:1–16:32, Macmillan, Indianapolis, Indiana, 1961.
- Intergovernmental Panel on Climate Change (IPCC), *Climate Change 1995: The Science of Climate Change, Contribution of Working Group I to the Second Assessment Report of the Intergovernmental Panel on Climate Change*, edited by J. T. Houghton et al., Cambridge Univ. Press, New York, 1996.
- Karl, T. R., P. D. Jones, R. W. Knight, G. Kukla, N. Plummer, V. Razuvayev, K. P. Gallo, J. Lindsey, R. J. Charlson, and T. C. Peterson, A new perspective on recent global warming: Asymmetry trends in daily maximum and minimum temperature, *Bull. Am. Meteorol. Soc.*, *74*, 1007–1023, 1993.
- Kasibhatla, P., W. L. Chameides, and J. St. John, A three-dimensional global model investigation of the seasonal variation in the atmospheric burden of anthropogenic sulfate aerosols, *J. Geophys. Res.*, *102*, 3737–3759, 1997.
- Kato, S., T. P. Ackerman, E. E. Clothiaux, and J. H. Mather, Optimum correlated- k distributions for a short-wave radiative transfer model, in *Current Problems in Atmospheric Radiation: Proceedings of the International Radiation Symposium*, pp. 301–304, A. Deepak, Hampton, Va., 1997.
- Kattawar, G. W., and G. N. Plass, Electromagnetic scattering from absorbing spheres, *Appl. Opt.*, *6*, 1377–1382, 1967.
- Key, J., Streamer user's guide, 71 pp., Coop. Inst. for Res. in Environ. Sci., Univ. of Colo., Boulder, 1994.
- Kiehl, J. T., and B. P. Briegleb, The relative roles of sulfate aerosols and greenhouse gases in climate forcing, *Science*, *260*, 311–314, 1993.
- Kneizys, F. X., E. P. Shettle, W. O. Gallery, J. H. Chetwynd Jr., L. W. Abreu, J. E. A. Selby, R. W. Fenn, and R. A. McClatchey, Atmospheric transmittance/radiance: Computer code LOWTRAN 5, *Rep. AFGL-TR80-0067*, 233 pp., Air Force Geophys. Lab., Bedford, Mass., 1980.
- Kneizys, F. X., E. P. Shettle, L. W. Abreu, J. H. Chetwynd, G. P. Anderson, W. O. Gallery, J. E. A. Selby, and S. A. Clough, User's guide to LOWTRAN 7, *Rep. AFGL-TR88-0177*, Air Force Geophys. Lab., Bedford, Mass., 1988.
- Lacis, D., and J. E. Hansen, A parameterization for the absorption of solar radiation in the Earth's atmosphere, *J. Atmos. Sci.*, *31*, 118–133, 1974.
- Lacis, A. A., and M. I. Mishchenko, Climate forcing, climate sensitivity, and climate response: A radiative modeling perspective on atmospheric aerosols, in *Aerosol Forcing of Climate*, edited by R. J. Charlson and J. Heintzenberg, pp. 11–42, John Wiley, New York, 1995.
- Langner, J., and H. Rodhe, A global three-dimensional model of the tropospheric sulfur cycle, *J. Atmos. Chem.*, *13*, 225–263, 1991.
- Laszlo, I., Calculation of longwave radiance spectra at a high resolution: Clear-sky results, in *Passive Infrared Remote Sensing of Clouds and the Atmosphere II*, edited by D. K. Lynch, *Proc. SPIE Int. Soc. Opt. Eng.* *2309*, 197–204, 1994.
- Liou, K. N., *An Introduction to Atmospheric Radiation*, 392 pp., Academic, San Diego, Calif., 1989.
- McClatchey, R. A., R. W. Fenn, J. E. A. Selby, F. E. Volz, and J. S. Garing, Optical properties of the atmosphere, 3rd ed., *Environ. Res. Pap. 411*, Air Force Cambridge Res. Lab., Hanscom Air Force Base, Mass., 1972.
- Neckel, H., and D. Labs, The solar radiation between 3300 and 12500 Å, *Solar Phys.*, *90*, 205–258, 1984.
- Nemesure, S., R. Wagener, and S. E. Schwartz, Direct short-wave forcing of climate by anthropogenic sulfate aerosol: Sensitivity to particle size, composition, and relative humidity, *J. Geophys. Res.*, *100*, 26,105–26,116, 1995.
- Oh, J. H., Physically-based general circulation model parameterization of clouds and their radiative interaction, Ph.D. dissertation, Department of Atmospheric Sciences, Oregon State University, Corvallis, OR, 315 pp., 1989.
- Ouimette, J. R., and R. C. Flagan, The extinction coefficient of multicomponent aerosols, *Atmos. Environ.*, *16*, 2405–2419, 1982.
- Penner, J. E., R. J. Charlson, J. M. Hales, N. S. Laulainen, R. Leifer, T. Novakov, J. Ogren, L. F. Radke, S. E. Schwartz, and L. Travis, Quantifying and minimizing uncertainty of climate forcing by anthropogenic aerosols, *Bull. Am. Meteorol. Soc.*, *75*, 375–400, 1994.
- Pham, M., J.-F. Müller, G. Brasseur, C. Granier, and G. Mégie, A three-dimensional study of the tropospheric sulfur cycle, *J. Geophys. Res.*, *100*, 26,061–26,092, 1995.
- Pilinis, C., S. N. Pandis, and J. H. Seinfeld, Sensitivity of direct climate forcing by atmospheric aerosols to aerosol size and composition, *J. Geophys. Res.*, *100*, 18,739–18,754, 1995.
- Plass, G. N., G. W. Kattawar, and F. E. Catchings, Matrix-operator-theory of radiative transfer, *Appl. Opt.*, *12*, 314–329, 1973.
- Press, W. H., B. P. Flannery, S. A. Teukolsky, and W. T. Vetterling, *Numerical Recipes*, 1st ed., Cambridge Univ. Press, New York, 1988.
- Ramaswamy, V., and S. M. Freidenreich, Solar radiative line-by-line determination of water vapour absorption and water cloud extinction in inhomogeneous atmospheres, *J. Geophys. Res.*, *96*, 9133–9157, 1991.
- Rothman, L. S., R. R. Gamache, A. Barbe, A. Goldman, J. R. Gillis, L. R. Brown, R. A. Toth, J. M. Flaud, and C. Camy-Peyret, AFGL atmospheric line parameters compilation: 1982 edition, *Appl. Opt.*, *22*, 2247–2256, 1983.
- Rothman, L. S., et al., The HITRAN molecular database: Editions of 1991 and 1992, *J. Quant. Spectrosc. Radiat. Transfer*, *48*, 469–508, 1992.
- Schwartz, S. E., The whitehouse effect: Shortwave radiative forcing of climate by anthropogenic aerosols, an overview, *J. Aerosol Sci.*, *27*, 359–382, 1996.
- Schwartz, S. E., and M. O. Andreae, Uncertainty in climate change caused by anthropogenic aerosols, *Science*, *272*, 1121–1122, 1996.
- Stackhouse, P. W., Jr., and G. L. Stephens, A theoretical and observational study of the radiative properties of cirrus: Results from FIRE 1986, *J. Atmos. Sci.*, *48*, 2044–2059, 1991.
- Stamnes, K., S.-C. Tsay, W. Wiscombe, and K. Jayaweera, Numerically stable algorithm for discrete-ordinate-method radiative transfer in multiple scattering and emitting layered media, *Appl. Opt.*, *27*, 2502–2509, 1988.
- Tang, I. N., and H. R. Munkelwitz, Simultaneous determination of refractive index and density of an evaporating aqueous solution droplet, *Aerosol Sci. Technol.*, *15*, 201–207, 1991.
- Tang, I. N., and H. R. Munkelwitz, Water activities, densities and refractive indices of aqueous sulfate and nitrate droplets of atmospheric importance, *J. Geophys. Res.*, *99*, 18,801–18,808, 1994.
- Toon, O. B., and T. P. Ackerman, Algorithms for the calcu-

- lations of scattering by stratified spheres, *Appl. Opt.*, **20**, 3657–3660, 1981.
- Toon, O. B., C. P. McKay, and T. P. Ackerman, Rapid calculation of radiative heating rates and photodissociation rates in inhomogeneous multiple scattering atmosphere, *J. Geophys. Res.*, **94**, 16,287–16,301, 1989.
- Tsay, S.-C., K. Stamnes, and K. Jayaweera, Radiative energy budget in the cloudy and hazy Arctic, *J. Atmos. Sci.*, **46**, 1002–1018, 1989.
- Twomey, S., *Atmospheric Aerosols*, 302 pp., Elsevier Sci., New York, 1977.
- Vermote, E. F., D. Tanré, J.-L. Deuzé, M. Herman, and J.-J. Morcrette, Second simulation of the satellite signal in the solar spectrum: An overview, *IEEE Trans. Geosci. Remote Sens.*, **35**, 675–686, 1997.
- Wagner, R. W., S. Nemesure, and S. Schwartz, Comparison of seasonal and zonal patterns of the direct and indirect radiative forcing of climate by aerosols, in *Fourth International Aerosol Conference, Abstracts*, edited by R. C. Flagan, Amer. Assoc. for Aerosol Res., pp. 556–557, 1994.
- Wiscombe, W. J., Mie scattering calculations: Advances in technique and fast, vector-speed computer codes, *Tech. Note NCAR/TN-140+STR*, Natl. Cent. for Atmos. Res., Boulder, Colo., 1979.
- Wiscombe, W., Improved Mie scattering algorithms, *Appl. Opt.*, **19**, 1505–1509, 1980.
- Wiscombe, W. J., and G. W. Grams, The backscattered fraction in two-stream approximations, *J. Atmos. Sci.*, **33**, 2440–2451, 1976.
- Wiscombe, W. J., R. M. Welch, and W. D. Hall, The effects of very large drops on cloud absorption, I, Parcel models, *J. Atmos. Sci.*, **41**, 1336–1355, 1984.
- World Climate Research Programme, Report of the expert meeting on aerosols and their climatic effects, *Rep. WCP 55*, 107 pp., World Meteorol. Org., Geneva, Switzerland, 1983.
- Zdunkowski, G. W., R. M. Welch, and G. Korb, An investigation of the structure of typical two-stream methods for the calculation of solar fluxes and heating rates in clouds, *Contrib. Atmos. Phys.*, **53**, 147–166, 1980.
- T. P. Ackerman, Meteorology Department, The Pennsylvania State University, 503 Walker Building, University Park, PA 16802. (e-mail: ackerman@essc.psu.edu)
- T. L. Anderson, Joint Institute for the Study of the Atmosphere and the Oceans, University of Washington, Box 351640, Seattle, WA 98195–1640. (e-mail: tadand@atmos.washington.edu)
- B. Bergstrom and P. Russell, NASA Ames Research Center, MS-245-5, Moffett Field, CA 94035-1000. (e-mail: bergstro@sky.arc.nasa.gov; prussell@mail.arc.nasa.gov)
- B. Bonnel, O. Boucher, and Y. Fouquart, Laboratoire d'Optique Atmosphérique, Université de Lille-I, 59655 Villeneuve d'Ascq Cedex, France. (e-mail: bonnel@loa.univ-lille1.fr; boucher@loa.univ-lille1.fr; fouquart@loa.univ-lille1.fr)
- P. Chylek, Q. Fu, M. Wang, and J. Wong, Atmospheric Science Program, Department of Physics, Dalhousie University, Halifax Nova Scotia, Canada B3H 3J5. (e-mail: chylek@atm.dal.ca; qfu@atm.dal.ca; muyin@atm.dal.ca; jwong@atm.dal.ca)
- A. Dahlback, Department of Physics, University of Oslo, P.O. Box 1048 - Blindern, 0316 Oslo, Norway. (e-mail: arne.dahlback@fys.uio.no)
- R. N. Halthore, S. Nemesure, S. Schwartz, Environmental Chemistry Division, Brookhaven National Laboratory, P.O. Box 5000, Upton, NY 11973-5000. (e-mail: halthore@bnl.gov; nemesure@bnl.gov; ses@bnl.gov)
- J. M. Haywood, Meteorological Research Flight, Y46 Building, Defence and Evaluation Research Agency, Farnborough, Hants GU14 0LX, England, U. K. (e-mail: jmhaywood@meto.gov.uk)
- T. Iversen and A. Kirkevåg, Department of Geophysics, University of Oslo, P.O. Box 1022 - Blindern, 0315 Oslo, Norway. (e-mail: trond.iversen@geofysikk.uio.no; alf.kirkevag@geofysikk.uio.no)
- S. Kato, Langley Research Center, Mail Stop 420, Hampton, VA 23681-0001. (e-mail: kato@aerosol.larc.nasa.gov)
- S. Kinne, NASA Goddard Space Flight Center, Code 923, Greenbelt, MD 20771. (e-mail: kinne@spamer.gsfc.nasa.gov)
- K. R. Knapp and G. L. Stephens, Department of Atmospheric Science, Colorado State University, Fort Collins, CO 80523. (e-mail: knapp@cira.colostate.edu; stephens@langley.atmos.colostate.edu)
- A. Lacis and M. I. Mishchenko, NASA Goddard Institute for Space Studies, 2880 Broadway, New York, NY 10025. (e-mail: alacis@giss.nasa.gov; mmishchenko@giss.nasa.gov)
- I. Laszlo, Department of Meteorology, University of Maryland, College Park, MD 20742. (e-mail: laszlo@atmos.umd.edu)
- V. Ramaswamy, NOAA Geophysical Fluid Dynamics Laboratory, Princeton University, P.O. Box 308, Princeton, NJ 08542. (e-mail: vr@gfdl.gov)
- D. L. Roberts, Hadley Centre for Climate Prediction and Research, Meteorological Office, London Road, Bracknell, Berkshire RG12 2SY, England, U. K. (e-mail: dlroberts@meto.gov.uk)
- M. E. Schlesinger and F. Yang, Department of Atmospheric Sciences, University of Illinois at Urbana-Champaign, 105 South Gregory Avenue, Urbana, IL 61801. (e-mail: schlesin@atmos.uiuc.edu; fanglin@atmos.uiuc.edu)
- R. Wagner, Analytical Sciences Division, Brookhaven National Laboratory, P.O. Box 5000, Upton, NY 11973-5000. (e-mail: wagner@bnl.gov)

(Received October 31, 1997; revised March 17, 1998; accepted March 19, 1998.)